Applied Surface Science 338 (2015) 75–84

Contents lists available at ScienceDirect

Applied Surface Science

journal homepage: www.elsevier.com/locate/apsusc

Direct in situ activation of Ag^0 nanoparticles in synthesis of Ag/TiO_2 and its photoactivity

N.F. Jaafar[a], A.A. Jalil[b,c,*], S. Triwahyono[a,d], J. Efendi[e], R.R. Mukti[f], R. Jusoh[c], N.W.C. Jusoh[c], A.H. Karim[a], N.F.M. Salleh[c], V. Suendo[f]

[a] Department of Chemistry, Faculty of Science, Universiti Teknologi Malaysia, 81310 UTM Johor Bahru, Johor, Malaysia
[b] Institute of Hydrogen Economy, Universiti Teknologi Malaysia, 81310 UTM Johor Bahru, Johor, Malaysia
[c] Department of Chemical Engineering, Faculty of Chemical Engineering, Universiti Teknologi Malaysia, 81310 UTM Johor Bahru, Johor, Malaysia
[d] Ibnu Sina Institute for Fundamental Science Studies, Universiti Teknologi Malaysia, 81310 UTM Johor Bahru, Johor, Malaysia
[e] Department of Chemistry, Universitas Negeri Padang, Jl. Prof. Hamka, Air Tawar, Padang, West Sumatera, Indonesia
[f] Division of Inorganic and Physical Chemistry, Faculty of Mathematics and Natural Science, Institut Teknologi Bandung, Jl Ganesha No. 10, Bandung 40132, Indonesia

ARTICLE INFO

Article history:
Received 9 January 2015
Received in revised form 10 February 2015
Accepted 16 February 2015
Available online 20 February 2015

Keywords:
$Ag–TiO_2$ catalyst
Electrochemical
Electron–hole pairs separation
Photodegradation
2-Chlorophenol

ABSTRACT

Metallic Ag nanoparticles (Ag^0) were successfully activated using a direct in situ electrochemical method before being supported on TiO_2. Catalytic testing showed that 5 wt% $Ag–TiO_2$ gave the highest photodegradation (94%) of 50 mg L^{-1} 2-chlorophenol (2-CP) at pH 5 using 0.375 g L^{-1} catalyst within 6 h, while under similar conditions, 1 wt% and 10 wt% $Ag–TiO_2$ only gave 75% and 78% degradation, respectively. Characterization results illustrated that the photoactivity was affected by the amount of Ag^0 and oxygen vacancies which act as an electrons trap to enhance the electron–hole separation. While, the Ag—O—Ti bonds formation reduced the photoactivity. The degradation followed a pseudo-first order Langmuir–Hinshelwood model where adsorption was the controlling step. Study on the effect of scavengers showed that the hole (H^+) and hydroxyl radical ($OH^•$) play important roles in the photodegradation. The regenerated photocatalyst was still stable after five cycling runs.

1. Introduction

Hazardous chlorinated phenolic compounds are continuously introduced into the environment through domestic and industrial activities, thus representing a severe toxicological risk [1]. Among these compounds, 2-chlorophenol (2-CP), which is widely used in the pulp, paper, biocide, cleaning agent, dye, preservative and pesticide industries, is known to have high toxicity and is also non-biodegradable [2,3]. Therefore, in order to eliminate this harmful pollutant from the environment, there are continuing studies on appropriate abatement methods such as wet oxidative, ozonation, oxidation degradation, hydrodechlorination, immobilization, and membrane [4–6]. However, these methods experience a few weaknesses such as generating secondary products and producing large amounts of sludge, in addition to being costly and time consuming [7–9]. Advanced oxidation processes (AOPs), which usually use a heterogeneous photocatalyst semiconductor, have become a popular method for the removal of this recalcitrant pollutant [10–12]. In the presence of suitable light irradiation and a specific catalyst, the hydroxyl radicals ($•OH$) formed in the oxidation process become the most important species in mineralizing the targeted pollutant into stable inorganic compounds such as carbon dioxide and water [13].

Various semiconductors have been used such as TiO_2, ZnO, SnO, α-Fe_2O_3, CdS, and ZnS [14–16]. Among them, TiO_2 shows better potential due to its strong oxidizing power, chemical-inertness and long-term stability against photo and chemical corrosion. However, photocatalytic application of TiO_2 has been limited by its high photogenerated electron–hole recombination rate, which hinders photocatalytic efficiency. In order to overcome this shortcoming, many strategies have been exploited including loading noble metals such as Au, Ag, Pt, and Pd to constrain charge carrier recombination and also act as electron acceptors [17]. Among them, Ag is the most potential photocatalyst used in doping TiO_2, due to its property of delaying the recombination of photogenerated electron–hole pairs, besides being less expensive compared with

* Corresponding author at: Department of Chemical Engineering, Faculty of Chemical Engineering, Universiti Teknologi Malaysia, 81310 UTM Johor Bahru, Johor, Malaysia. Tel.: +60 7 5535581; fax: +60 7 5588166.
E-mail address: aishah@cheme.utm.my (A.A. Jalil).

http://dx.doi.org/10.1016/j.apsusc.2015.02.106
0169-4332/

other noble metals [18]. The deposition of metallic Ag nanoparticles (Ag^0) onto TiO_2 may improve photocatalytic activity by facilitating effective charge separation that prevents rapid electron–hole recombination [19]. In addition, photocatalysts consisting of Ag^0 nanoparticles are more attractive than Ag halides due to the instability of Ag halides caused by photolysis, while Ag^0 nanoparticles manage to smooth the separation of electron–hole pairs [20].

Indeed, various methods have used to synthesize Ag^0 nanoparticles on TiO_2 supports by reducing Ag^+ to the metallic form, including heat-induced reduction, reducing agents, photoreduction, ionic liquids and UV or gamma ray methods [21–23]. However, these methods require either high temperature or a long reaction time to obtain the metallic Ag. Thus, it is necessary to find a simple and rapid synthesis method to obtain the Ag^0. Previously, we reported a simple in situ electrochemical method for preparing various metal nanoparticles such as α-Fe_2O_3, ZnO, ZrO_2, and CuO supported on zeolites [24–28]. Besides the formation of metallic nanoparticles, the incorporated metal ions in the support were also discovered during the electrolysis, resulting in photocatalysts with high potential for efficient decolorization of various dyes. Therefore, as an extension of the study, herein we report preparing Ag supported on TiO_2 using a similar in situ electrochemical method and its photoactivity toward degradation of 2-CP. The properties of the catalysts were characterized in detail by XRD, FT-IR, Raman, UV–vis DRS, photoluminescence, surface area analysis, TEM, FESEM-EDX and cyclic voltammetry. We believe these new findings on a simple preparation method for the formation of metallic Ag supported on TiO_2 in tandem with incorporation of the Ag into the TiO_2 structure could contribute to photodegradation strategies for various organic pollutants as well as other reactions. The photocatalytic performance, kinetic studies, proposed mechanism and reusability of the catalysts are also discussed.

2. Experimental

2.1. Reagents, material and apparatus

The TiO_2 powder catalyst JRC-TiO_2-2 was supplied by the Catalysis Society of Japan. The Ag and Pt plates of greater than 99% purity were used as electrodes and were obtained from Nilaco, Japan. *N*,*N*-Dimethylformamide (DMF), perchloric acid and hydrochloric acid were purchased from MERCK, Malaysia and acetone was purchased from HmbG Chemical. Naphthalene and tetraethylammonium bromide solution were obtained from Fluka Chemical and methanol was purchased from RPE Reagent pure Erba. Silver nitrate ($AgNO_3$), sodium hydroxide (NaOH) and hydrochloric acid (HCl) were purchased from QREC™ and 2-CP from Alfa Aesar, Germany with 99% purity. Ammonium oxalate (AO) was obtained from Riedel-De Haen AG Seelze-Hannover while isopropanol (IP) was supplied by System®. Tetraethylammonium perchlorate (TEAP), which was used as a supporting electrolyte in the electrolysis was prepared accordance with the procedure reported in the literature [29].

2.2. Preparation of catalyst

Metallic Ag and Ag–TiO_2 catalyst were prepared by an electrolysis method in accordance with the procedure reported in the literature [30] (S1.1 and S1.2). The 1, 5, and 10 wt% Ag loaded onto TiO_2 were prepared by adjusting the electrolysis time according to the Faraday's law. For comparison on catalytic performance, the 5 wt% Ag–TiO_2 was also prepared by a photodeposition method (S1.3).

2.3. Characterization

The crystalline structures of the catalysts were carried out using a Bruker Advance D8 X-ray powder diffractormeter (XRD) with Cu Kα radiation (λ = 1.5418 Å) at 2θ angle ranging from 20° to 90°. The morphological properties of the catalysts were examined by Transmission electron microscopy (TEM, JEOL JEM-2100F). The catalysts were ultrasonically dispersed in acetone and deposited on amorphous, holey carbon membranes. Field-Emission Scanning Electron Microscopy was conducted to determine elemental composition of samples using Energy Dispersion X-ray Spectroscopy (FESEM-EDX, JEOL JSM-6701F). UV–vis diffuse reflectance spectra (UV–vis DRS) were recorded in air at room temperature over a range of wavelengths from 250 to 500 nm using a Perkin Elmer Lambda 900 UV/vis/NIR spectrometer with an integrating sphere. The chemical functional groups present in the catalysts were identified by FT-IR spectroscopy (Perkin Elmer Spectrum GX FTIR Spectrometer). IR absorbance data were obtained over a range of wavenumbers from 395 to 4000 cm^{-1}.

Nitrogen adsorption–desorption isotherms were used to determine the textural properties at liquid nitrogen temperatures using a Micromeritics ASAP 2010 instrument. The Brunnauer–Emmett–Teller (BET) and non-local density functional theory (NLDFT) methods were used to calculate surface area and pore distribution, respectively. Prior to measurement, all of the samples were degassed at 110 °C and 0.1 Pa. Raman spectrometer were recorded using Bruker Senterra at room temperature using 10 mW for excitation from 785 nm laser diode with the acquisition times were 10 s with 2 time repeat. The photoluminescence (PL) (JASCO Spectrofluorometer) (FP-8500) with 150 W Xe lamp as excitation source was used to determine the photochemical properties, electronic structure and optical of the catalysts.

A conventional three-electrode electrochemical cell was used for the CV measurements, with a high surface area Pt counter electrode and Ag/AgCl was used as reference electrode, powered by a DY2113 potentiostat voltammetric analyser (Digi-Ivy, Inc.). The isoelectric point (pH_{ZPC}) of the catalyst was performed using powder addition (PA) method (S2), as described in the literature [14].

2.4. Photodegradation of 2-chlorophenol

The photoactivity of the catalysts was tested on the degradation of 2-CP. The photocatalytic experiments were performed in a batch reactor fixed with UV lamp (4 × 9 W; 254 nm) and cooling system. A 0.375 g L^{-1} catalyst was added to 200 mL 2-CP solution with a desired concentration and stirred for 1 h in the dark to achieve adsorption–desorption equilibrium before being exposed to light radiation for 6 h. To ensure the accuracy, each set of experiment was performed three times. The initial pH and concentration of 2-CP solution were at pH = 5 and 50 mg L^{-1}, respectively (S3).

3. Result and discussion

3.1. Physicochemical properties of the prepared catalyst

The XRD patterns of metallic Ag, TiO_2 and Ag–TiO_2 with different levels of Ag loading are shown in Fig. 1. A series of characteristic peaks was observed for Ag^0 at 38.12° (1 1 1), 44.31° (2 0 0), 64.45° (2 2 0), 77.41° (3 1 1) and 81.55° (2 2 2) (Fig. 1A and B/a) that was consistent with peaks typical of metallic silver (JCPDS file no. 01-087-0717). Fig. 1B/b shows the diffraction peaks of the TiO_2 anatase phase (JCPDS file no. 00-004-0477) with peaks at 25.4° (1 0 1), 36.9° (1 0 3), 37.8° (0 0 4), 38.5° (1 1 2), 48.2° (2 0 0), 53.9° (1 0 5), 55.3° (2 1 1), and 63.2° (2 0 4). The XRD patterns of the Ag–TiO_2 catalysts (Fig. 1B/c–e) were similar to those of TiO_2 alone (Fig. 1B/b),

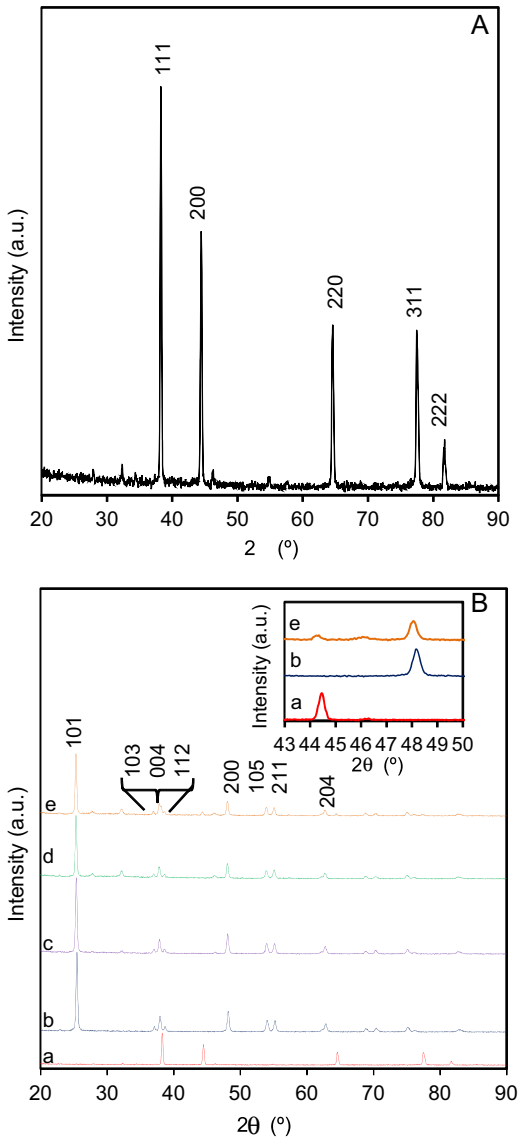

Fig. 1. XRD diffractograms of (A) metallic Ag prepared by electrochemical method; and (B) (a) metallic Ag, (b) TiO_2, (c) 1 wt% Ag–TiO_2, (d) 5 wt% Ag–TiO_2 and (e) 10 wt% Ag–TiO_2. Insert figure shows the XRD diffractogram at 2θ = 43–50°.

indicating the introduction of Ag did not have much of an effect on the structure of the catalyst [28]. However, the peak intensity of TiO_2 seemed to decrease with increasing Ag loading. This was most probably due to the good distribution of Ag on the surface of the TiO_2 [31]. Diffraction spectra of Ag distributed on the TiO_2 could not be observed in either the 1 or the 5 wt% Ag–TiO_2 catalysts. The diffraction spectrum of Ag was clearly observed on the 10 wt% Ag–TiO_2 (inset Fig. 1B/e), which showed a weak peak at 2θ = 44.5°, signifying the Ag^0 particles were widely dispersed on the TiO_2 support [32]. In addition, increasing Ag loading seemed to shift the TiO_2 diffraction peak at (1 0 1) toward a slightly lower angle, from 25.44° to 25.30° (figure not shown). This phenomenon is most probably due to the introduction of Ag causing shrinkage of some of the TiO_2 crystallite planes, resulting in disordering of the crystallinity of the TiO_2 [33,34]. In addition, the value of d_{101} was found to increase with increasing Ag loading, also suggesting an interaction between Ag and TiO_2 (Table 1). The particle sizes of the Ag^0 and TiO_2 were found to be 37 and 31 nm, respectively, which were calculated by the Debye–Scherrer equation (S4) based on the major peak at 2θ = 38.12° (1 1 1) for Ag^0 (Fig. 1A), and at 2θ = 25.35° (1 0 1) for TiO_2 (Fig. 1B/b).

The adsorption branches of the isotherm for pore size distribution of the catalysts were derived by the NLDFT method and the results are shown in Fig. 2. Fig. 2A shows the pore distribution of Ag^0, which demonstrate that its pore diameter was in the range of 1.56–7.59 nm with an average of 3.66 nm. The inset figure in Fig. 2A shows the pore distribution of TiO_2. It was observed that the Ag–TiO_2 catalysts illustrated multiple pore size distributions, with two major peaks at 3.66 and 32.7 nm, representing the pore diameters of the Ag^0 and TiO_2, respectively (Fig. 2B). Increasing the loading of Ag onto TiO_2 increased the number of 3.66 nm pores while decreasing the 32.7 nm pores. The surface area and pore volume of the catalysts also decreased with increased Ag loading (Table 1), suggesting possible pore blockage on the TiO_2 [27]. The increase in pore size after the addition of 5 wt% Ag may due to the larger crystallites aggregating and merging some of the pores [21]. However, the pore size seemed to be drastically decreased by the addition of 10 wt% Ag, this may due to agglomerated Ag particles covering the TiO_2 pores.

The morphology and metal distribution of the catalysts were then examined by TEM and FESEM analyses, and the images are shown in Fig. 3. Fig. 3A shows a TEM image of TiO_2, indicating translucent, irregularly shaped particles in the range of 20–40 nm. A TEM image for 5 wt% Ag–TiO_2 is shown in Fig. 3B, in which the dark dots most probably represent Ag^0 nanoparticles that are well dispersed across the surface of TiO_2 and may also be incorporated into this support. A similar observation has been reported in the literature with regard to the incorporation of Ag nanocrystals into TiO_2 [35]. The FESEM image of 5 wt% Ag–TiO_2 catalyst and EDX mapping of Ag–TiO_2 catalysts with different Ag loadings are shown in Fig. 3D–F, respectively. Fig. 3C shows the irregular shapes of 5 wt% Ag–TiO_2, while the distribution of Ag particles on the surface of the TiO_2 is illustrated by the red dots in Fig. 3D–F, which seem to increase with increasing Ag loading. Fig 3F highlights a few spots of clustered red dots, signifying agglomerations of Ag^0 nanoparticles on the TiO_2 surface. This result supports the BET surface area analysis (Table 1), which showed the decrease in surface area with increasing Ag loading on TiO_2. It has also been reported in the literature that the atomic silver clusters were eliminated by aggregating into larger silver particles upon calcination at 773 K [32]. The insert tables in Fig. 3D–F confirm the percentage by weight of Ag loaded on the TiO_2, approximately 1, 5 and 10 wt%, respectively.

Table 1
Textural properties of catalysts.

Catalyst	Surface area (m^2/g)	Pore volume ($\times 10^{-2}$ cm^3/g)	Pore size (nm)	$d_{spacing}$ (Å)	Band gap (eV)[c]
Ag	0.75	0.49	3.78	2.35[a]	3.80
TiO_2	10.5	10.2	32.6	3.49[b]	3.30
1 wt% Ag–TiO_2	15.2	11.2	32.7	3.51[b]	3.30
5 wt% Ag–TiO_2	13.4	8.96	35.0	5.52[b]	3.30
10 wt% Ag–TiO_2	10.8	5.60	3.78	5.53[b]	3.30

[a] $d_{spacing}$ at (1 1 1).
[b] $d_{spacing}$ at (1 0 1).
[c] Band gap calculated using Kubelka–Munk (K–M) spectrum when plotting the $f_{K-M} = (hc/\lambda)^2$ vs. $h\nu$.

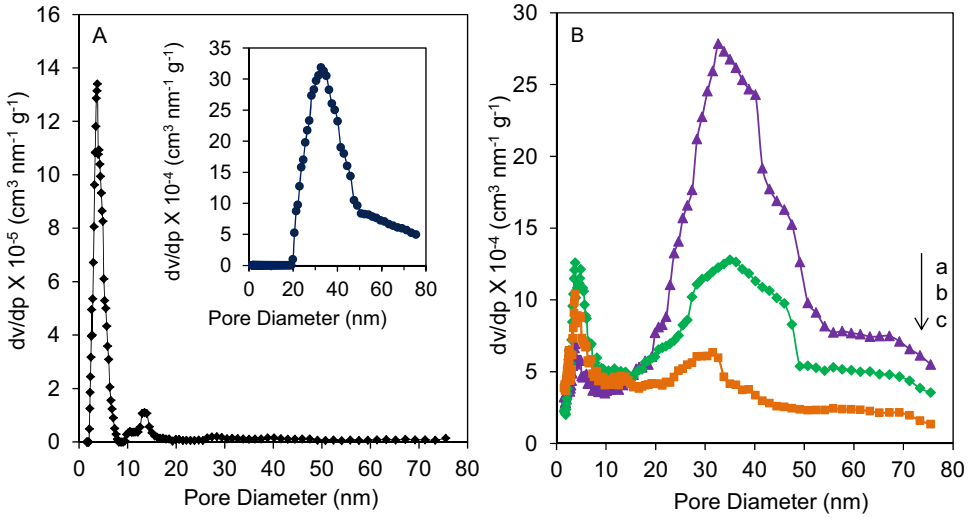

Fig. 2. (A) Pore distribution of the metallic Ag. Insert figure show the pore distribution of TiO_2; (B) Pore distribution of (a) 1 wt% Ag–TiO_2, (b) 5 wt% Ag–TiO_2 and (c) 10 wt% Ag–TiO_2.

The catalysts were then subjected to FT-IR analysis and the spectra are shown in Fig. 4A. Three moderate bands were observed at 3420, 2390, and 1604 cm^{-1} that are attributed to O—H stretching, CO_2, and the O—H bond of the hydroxyl group, respectively [36,37]. A strong band at 535 cm^{-1} was assigned to the Ti—O—Ti bond of the TiO_2 anatase phase. The intensity of this band decreased with increasing Ag loading, indicating possible disturbance of the TiO_2 framework by the Ag species [38]. Next, the catalysts' chemical bonds and symmetry molecules in the fingerprint region were further identified using Raman spectrometry (Fig. 4B and C). The bands at 624, 498, 382.5, 182, and 138.5 cm^{-1} are characteristic of the TiO_2 anatase phase, while no rutile phase was observed because characteristic bands at 605, 425, and 245 cm^{-1} were absent [39]. This result is in agreement with the XRD data. The Ti—O stretching mode was reflected in bands at 624 cm^{-1} (E_g) and 498 cm^{-1} (A_{1g}), while Ti—O—Ti bending type vibrations appeared at 382.5 cm^{-1} (B_{1g}) and 138.5 cm^{-1} (E_g) [40]. The addition of Ag decreased the TiO_2 band and also shifted the band at 138.5–143.5 cm^{-1}, signifying a resonant Raman effect due to the interaction between Ag and TiO_2 [41]. This result is in agreement with the FT-IR results, which indicated a possible interaction between the Ag and TiO_2. A band corresponding to Ag was not detected in the FT-IR spectra but, significantly, a new peak was observed in the Raman spectra at 97 cm^{-1} in the Ag–TiO_2 catalysts that corresponded to a Ag lattice vibration mode [42]. The intensity of these peaks was inversely proportional to the increasing Ag loading. These observations supported the XRD and FT-IR data and also changes in particle size determined by the Debye–Scherrer equation that confirmed the interaction between Ag and TiO_2. In order to define the actual structure of Ag–TiO_2, the broad band at 535 cm^{-1} was further confirmed by Gaussian curve-fitting to provide evidence of Ag^0 formation (Figs. S1 and S2).

The optical absorption properties of the catalysts were investigated using a UV–vis diffused reflectance spectral technique. Fig. S3A demonstrates that all the catalysts had absorption in the ultraviolet region, exhibiting a band edge at 350 nm, except for the Ag^0 spectrum that displayed an adsorption edge at 320 nm. The absorption bands below 370 nm was observed for TiO_2 and the Ag–TiO_2 catalysts, which assigned as charge-transfer from the valence band to the conduction band, while the Ti—O bond was detected in the UV region at 400–600 nm [43]. The band gap (Table 1) of Ag (3.8 eV) was higher compared to the Ag–TiO_2 catalyst (3.3 eV), verifying the band gap was reduced after being supported with TiO_2.

In order to confirm the synthesis route of the Ag–TiO_2 catalysts, the reduction of naphthalene was measured by cyclic voltammetry in 0.1 M TEAP-DMF using an Ag/AgCl reference electrode [44]. The result is shown in Fig. S3B. It was confirmed that the Ag^+ was reduced (Fig. S3B/b) subsequent to naphthalene (Fig. S3B/a) in the DMF solution. Thus, in parallel with previous studies [24,28,30], it is proposed that dissolved Ag ions from the Ag anode were reduced by the naphthalene radical anions produced at the cathode to form the zero-valence Ag (inset Fig. S3B). In addition, the Ag^+ might also undergo cation exchange with the Ti^{4+} to form Ti—O—Ag bonds as elucidated by the XRD, FT-IR and Raman data [25,28]. Thus, the novelty of the present work is related to the straight forward and simple electrochemical preparation method for Ag^0 nanoparticles as well as incorporation of the Ag ions within the TiO_2 support, which provides an optically interesting material.

3.2. Photocatalytic testing on the degradation of 2-chlorophenol

3.2.1. Performance of the catalysts

The photocatalytic performance of Ag^0, TiO_2 and 5 wt% Ag–TiO_2 was studied with respect to the degradation of 2-CP and the results are shown in Fig. 5. All catalysts were stirred for 1 h in the dark to achieve adsorption–desorption equilibrium before being exposed to UV-light radiation for 6 h (Fig. 5A). In order to compare the efficiency of Ag^0 supported on the TiO_2 prepared by the current in situ electrochemical method (IS), the 5 wt% Ag–TiO_2 were also prepared by the conventional photodeposition (PD) method, in which the Ag ions were reduced to Ag^0 under UV irradiation for 3 h subsequent to the addition of TiO_2 [23]. While, Fig. 5B shows the performance of all catalysts under dark and UV-light condition. It could be observed that all the catalysts showed better performance under UV-light irradiation compared to being in darkness. In addition, photocatalytic degradation under visible light (data not shown) resulted in a negligible decrease in the 2-CP concentration (<22%) during 6 h of irradiation, indicating the importance of UV-light to the reaction. Photocatalytic degradation of 2-CP using 5 wt% Ag–TiO_2 (IS) showed the highest percentage (94%), followed by 5 wt% Ag–TiO_2 (PD) (81%), TiO_2 (62%) and Ag (48.5%), signifying the importance of the synergistic effect of Ag and TiO_2 in the system. This result also demonstrated that the Ag–TiO_2 prepared by the current electrochemical method has higher activity compared to the PD method.

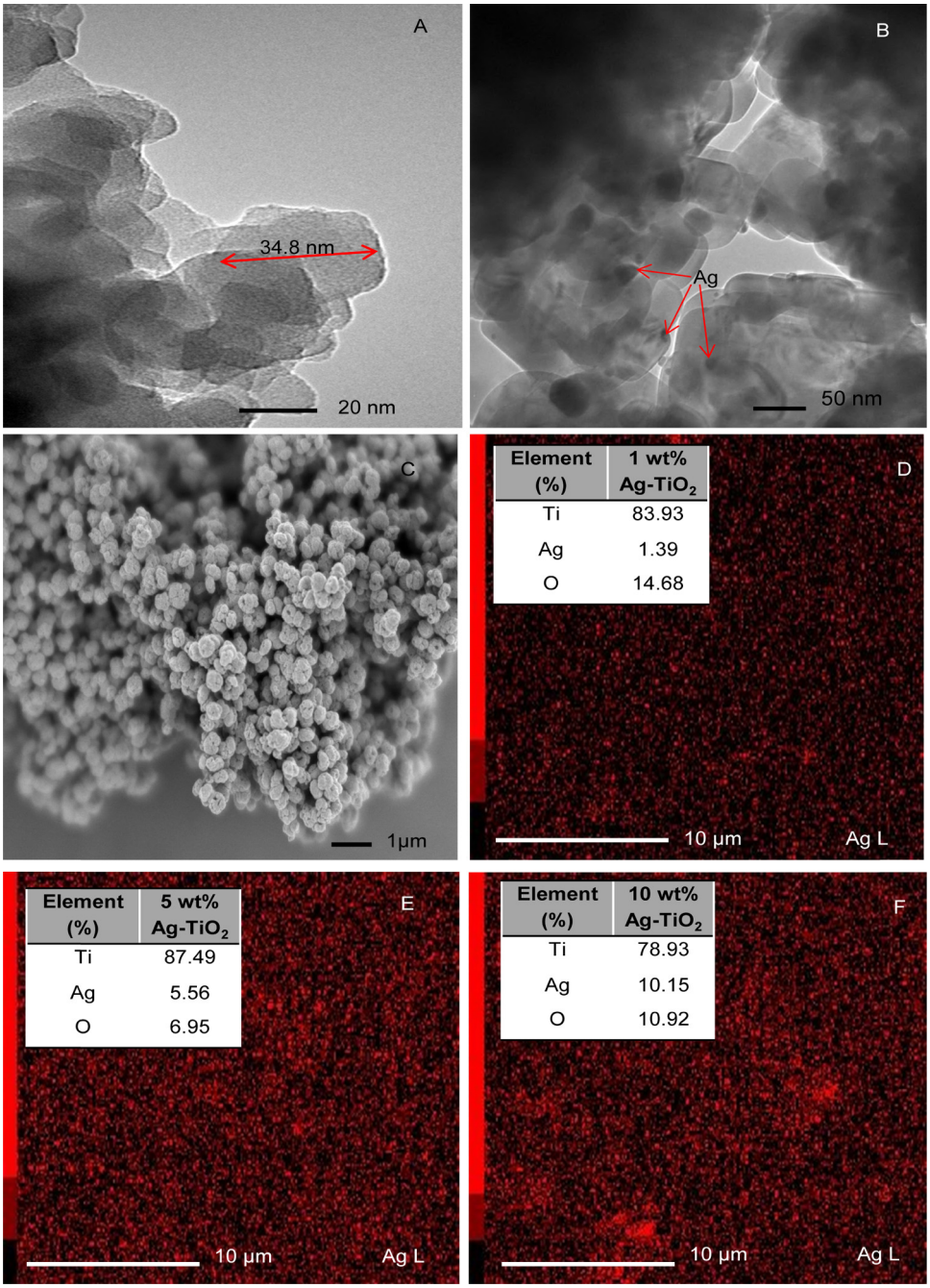

Fig. 3. TEM image of (A) TiO_2 and (B) 5 wt% Ag–TiO_2; FESEM image of (C) 5 wt% Ag–TiO_2; EDX mapping of Ag on (D) 1 wt% Ag–TiO_2, (E) 5 wt% Ag–TiO_2 and (F) 10 wt% Ag–TiO_2. Insert table shows elemental analysis of catalysts. (For interpretation of the references to color in the text, the reader is referred to the web version of the article.)

3.2.2. *Effect of pH and catalyst dosage*

The pH of solution is an important controlling parameter in evaluating an aqueous phase for photocatalytic reaction. In this study, the effect of pH on the degradation of 2-CP by 5 wt% Ag–TiO_2 was investigated by varying the pH values from 3 to 9. The results are presented in Fig. 6A. The greatest degradation was obtained at pH 5, with 94%, while degradation at pH 3, 7 and 9 was 75%, 67.9% and 67.3%, respectively. This result could be explained by the amphoteric performance of the catalyst, which is based on its zero point charge (pH_{ZPC}). The pH_{ZPC} was found to be at pH 6.3 (inset Fig. 6A); thus, below this pH value the catalyst surface would be positively charged and attracted the negatively charged 2-CP, and vice versa [45,46]. This may explain the highest degradation at acidic condition rather than alkaline.

The effect of 5 wt% Ag–TiO_2 catalyst dosage was also studied in the range of 0.19–0.75 g L^{-1} and the results are shown in Fig. 6B. Degradation of 2-CP was increased up to 94% with increasing catalyst dosage up to 0.375 g L^{-1}, but further addition of catalyst seemed reduce the degradation. This is because the higher the catalyst dosage, the higher the number of active sites that could absorbed more photons and 2-CP [26,47,48]. However, an excess dosage led to the turbidity of suspension in the solution, which reduced the light penetration and impeded the photocatalytic process [49].

3.2.3. *Effect of Ag loading on TiO_2*

The amount of Ag loading on TiO_2 was examined, ranging from 1 to 10 wt% (Fig. 7A). The 5 wt% was found to be the optimal amount of Ag loading, giving 94% degradation, while the capability of the

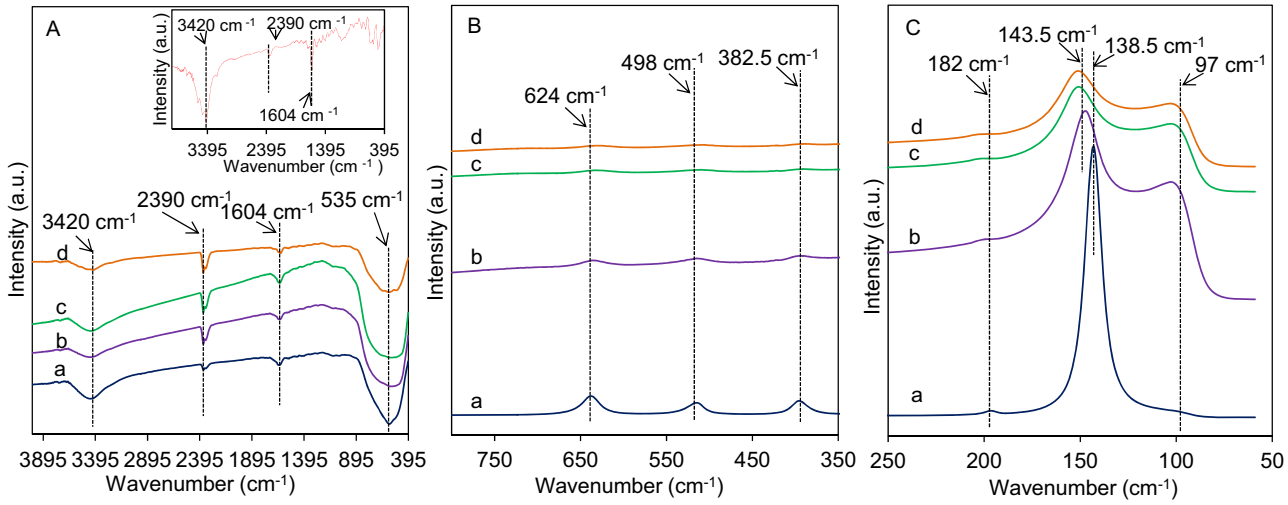

Fig. 4. (A) FT-IR spectra of (a) TiO_2, (b) 1 wt% Ag–TiO_2, (c) 5 wt% Ag–TiO_2 and (d) 10 wt% Ag–TiO_2. Insert figure shows the FT-IR spectra of metallic Ag; (B) and (C) Raman spectra of (a) TiO_2, (b) 1 wt% Ag–TiO_2, (c) 5 wt% Ag–TiO_2 and (d) 10 wt% Ag–TiO_2.

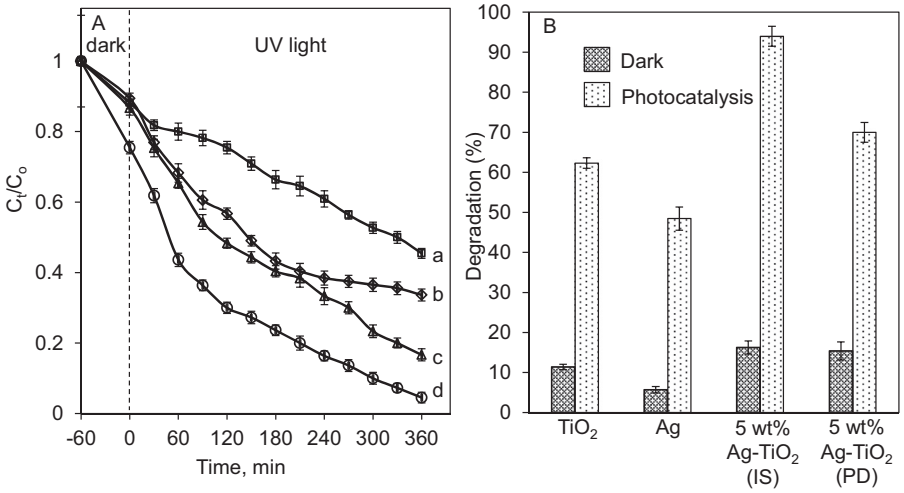

Fig. 5. (A) Catalytic performance of (a) metallic Ag, (b) TiO_2, (c) 5 wt% Ag–TiO_2 (PD) and (d) 5 wt% Ag–TiO_2 (IS) on degradation of 2-CP; (B) catalytic performance of the catalysts under dark and UV-light irradiation ($C_{2\text{-CP}}$ = 10 mg L^{-1}, pH = 5, W = 0.375 g L^{-1}, t = 6 h, 30 °C).

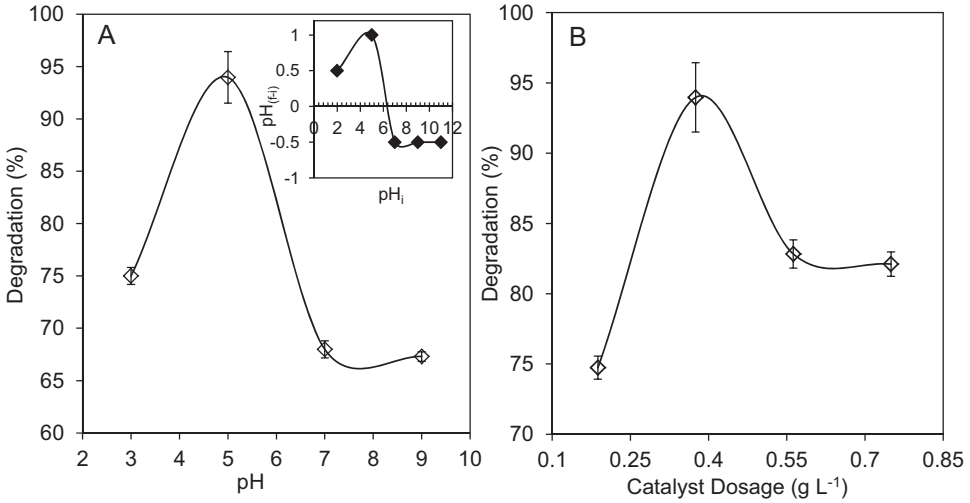

Fig. 6. (A) Effect of pH using 5 wt% Ag–TiO_2 on degradation of 2-CP. Insert figure shows the isoelectric point (pH_{ZPC}) of 5 wt% Ag–TiO_2; (B) effect of catalyst dosage using 5 wt% Ag–TiO_2 on degradation of 2-CP ($C_{2\text{-CP}}$ = 10 mg L^{-1}, pH = 5, W = 0.375 g L^{-1}, t = 6 h, 30 °C).

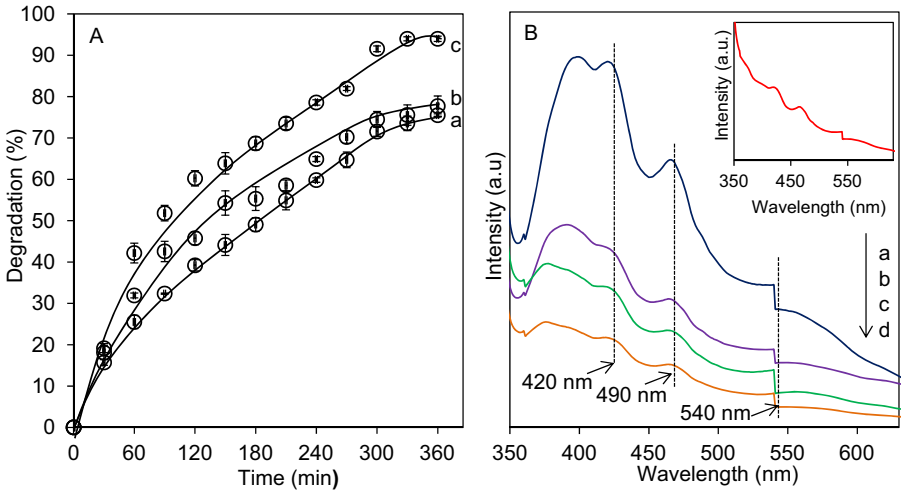

Fig. 7. (A) Effect of metallic Ag loading on TiO_2 for degradation of 2-CP (a) 1 wt% Ag–TiO_2, (b) 10 wt% Ag–TiO_2 and (c) 5 wt% Ag–TiO_2; (B) PL spectra of (a) TiO_2 (b) 1 wt% Ag–TiO_2 (c) 5 wt% Ag–TiO_2 and (d) 10 wt% Ag–TiO_2 with the excitation wavelength of 325 nm. Insert figure shows the PL spectra of metallic Ag ($C_{2\text{-CP}}$ = 10 mg L^{-1}, pH = 5, W = 0.375 g L^{-1}, t = 6 h, 30 °C).

catalysts was decreased both for 10 wt% (78%) and 1 wt% (75%). The charge separation of the TiO_2 improved with increased Ag loading may increase the rate of electron transfer to dissolved oxygen, resulting in better photocatalytic activity [50]. However, further addition of metallic Ag may act as a recombination center and it demonstrated by PL spectra (Fig. 7B). In addition, light penetration into the TiO_2 surface for 10 wt% Ag–TiO_2 might be less compared to 5 wt% Ag–TiO_2 due to agglomerated Ag particles blocking some of the TiO_2 pores (Fig. 2B), thus reducing the activity of the catalyst.

Fig. 7B shows PL spectra of the catalysts under the excitation wavelength of 325 nm. The intensity of the PL spectra of the parent TiO_2 catalysts decreased considerably with the addition of Ag, reflecting the enhanced charge pair separation that led to the increased photoactivity of the catalysts (Fig. 5) [51]. However, sometimes this phenomenon seems to be incompatible, wherein further addition of Ag^0 may act as a recombination center that is detrimental to the photocatalytic activity [40]. This may explain why the percent degradation of 10 wt% Ag–TiO_2 was less than that of 5 wt% Ag–TiO_2 (Fig. 7A). The band at 420 nm is attributed to the surface recombination transition, whereas the bands at 460 nm and 540 nm are corresponding oxygen vacancies [52]. It can be seen that the band intensity at 540 nm is much higher for 5 wt% Ag–TiO_2 compared to 1 wt% and 10 wt% Ag–TiO_2, indicating that 5 wt% Ag–TiO_2 has the greatest number of surface oxygen vacancies, which act as electron traps that inhibit the electron–hole pair recombination process [53]. In relation to the XRD, FT-IR and Raman results, 5 wt% Ag–TiO_2 contained the highest Ag^0 content compared to 1 wt% and 10 wt% Ag–TiO_2, which played the key role in the photodegradation. The smaller number of oxygen vacancies in 10 wt% Ag–TiO_2 could be explained by isomorphous substitution of Ag in the TiO_2 structure leading to occupancy of the TiO_2 surface as elucidated by the surface area analysis results (Table 1).

3.2.4. Kinetic studies

The degradation efficiency of the catalyst also depends on the initial concentration of the substrate. Table 2 demonstrates that the degradation of 2-CP was decreased with increasing initial concentration. An increase in initial concentration could inhibited light penetrating to the surface of the catalyst and thus reduced the formation of the hydroxyl radicals that play such an important role in the degradation. Herein, the degradation rates of 2-CP were also studied using the Langmuir–Hinshelwood (L–H) model [54] over 5 wt% Ag–TiO_2 catalyst and the linear plot of $\ln(C_0/C_t)$ vs. irradiation time are shown in Fig. 8. All the plots can be roughly fitted to a straight line, indicating the photocatalytic degradation followed pseudo-first-order kinetics models [24]. Table 2 shows that the k_{app} decreased with increasing initial concentration, demonstrating the system was favorable at low concentration [26]. The values of k_r (reaction rate constant) and K_{LH} (adsorption coefficient) were found to be 0.238 mg L^{-1} min^{-1} and 0.038 L mg^{-1}, respectively, signifying the adsorption of 2-CP was the controlling step in the process [28]. A comparison study on photodegradation of 2-CP over various photocatalysts tabulated in Table 3 clearly shows that the Ag–TiO_2 is quite comparable to other metal oxide catalysts.

3.2.5. Proposed reaction mechanism

In order to study the mechanism of the photodegradation, the importance of two active species, hole (H^+) and •OH were investigated by using AO and IP as scavenging agents, respectively [11].

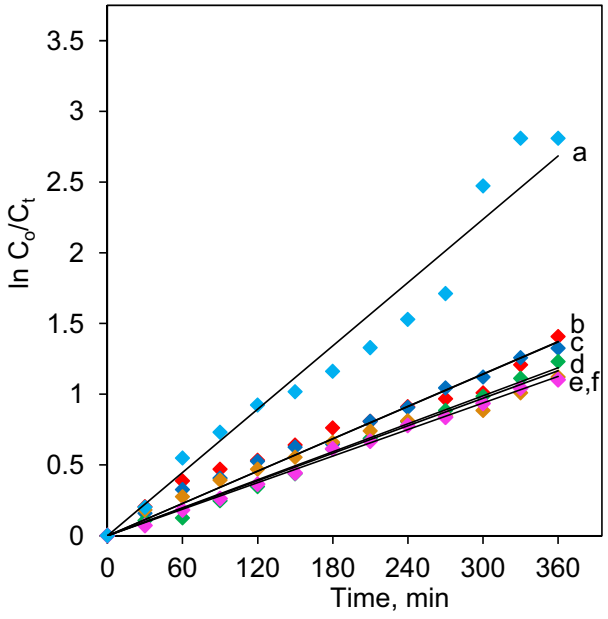

Fig. 8. Photodegradation kinetics of 2-CP using 5 wt% Ag–TiO_2 at different initial concentrations (a) 10 mg L^{-1}, (b) 20 mg L^{-1}, (c) 30 mg L^{-1}, (d) 50 mg L^{-1}, (e) 70 mg L^{-1} and (f) 100 mg L^{-1} (pH = 5, W = 0.375 g L^{-1}, t = 6 h, 30 °C).

Table 2
Percentage degradation at different initial concentrations of 2-CP and pseudo-first-order apparent constant values for 2-CP degradation using 5 wt% Ag–TiO_2 (pH = 5, W = 0.375 g L^{-1}, t = 6 h, 30 °C).

Initial 2-CP concentration, C_0	Degradation (%)	Reaction rate, k_{app} ($\times 10^{-3}$ min^{-1})	Initial reaction rate, r_0 ($\times 10^{-2}$ mg L^{-1} min^{-1})
10	94.0	7.5	7.5
20	75.5	3.8	7.6
30	73.5	3.5	10.5
50	70.8	3.3	16.5
70	67.4	3.1	21.7
100	66.7	2.8	28.0

Table 3
Comparison of photocatalytic activity of 2-CP over various catalysts.

Catalyst	2-CP initial conc. (mg L^{-1})	Dosage (g L^{-1})	Contact time (h)	Decolorization (%)	Ref.
$CS/CoFe_2O_4$	25	1.0	4	95.4	[55]
CNT/TiO_2	25	0.1	4	20	[56]
ZrO_2-doped $ZnCo_2O_4$	50	1.0	3	70	[57]
N-doped TiO_2	10	0.02	6	91	[58]
TiO_2	50	1.0	3	50.5	[59]
IL-FeOOH	50	0.30	8	85	[11]
Ag–TiO_2	10	0.375	6	94	This study

Both resulted in rather low degradation percentages of 64% and 72% (Fig. 9A) when using AO and IP, respectively, demonstrating the important role of H^+ and •OH in the degradation process. Consequently, the mechanism of the reaction is proposed to be as follows (Fig. 9B): UV-light irradiation leads to an excitation of electrons from the TiO_2 valence band (VB) to its conduction band (CB), leaving behind holes in the VB [60]. The photoexcited electrons in the CB are then transferred to the Ag^0 nanoparticles, leading to photon absorption because the Fermi level of Ag^0 is less than that TiO_2 [61]. At this time, the Schottky barrier was formed from the charge-transfer process between TiO_2 and Ag particles, which acts as an electron sink [40]. This barrier would improve the charge separation and inhibit electron–hole recombination, which then increases the concentration of photogenerated holes at the catalyst surface [19]. The trapped electrons on the Ag had good fluidity, participating in the reduction of O_2 molecules to produce superoxide anion radicals ($O_2^{\bullet -}$). The $O_2^{\bullet -}$ finally reacted with H^+ in the water to produce HOO• before generating the OH•, while the holes in the

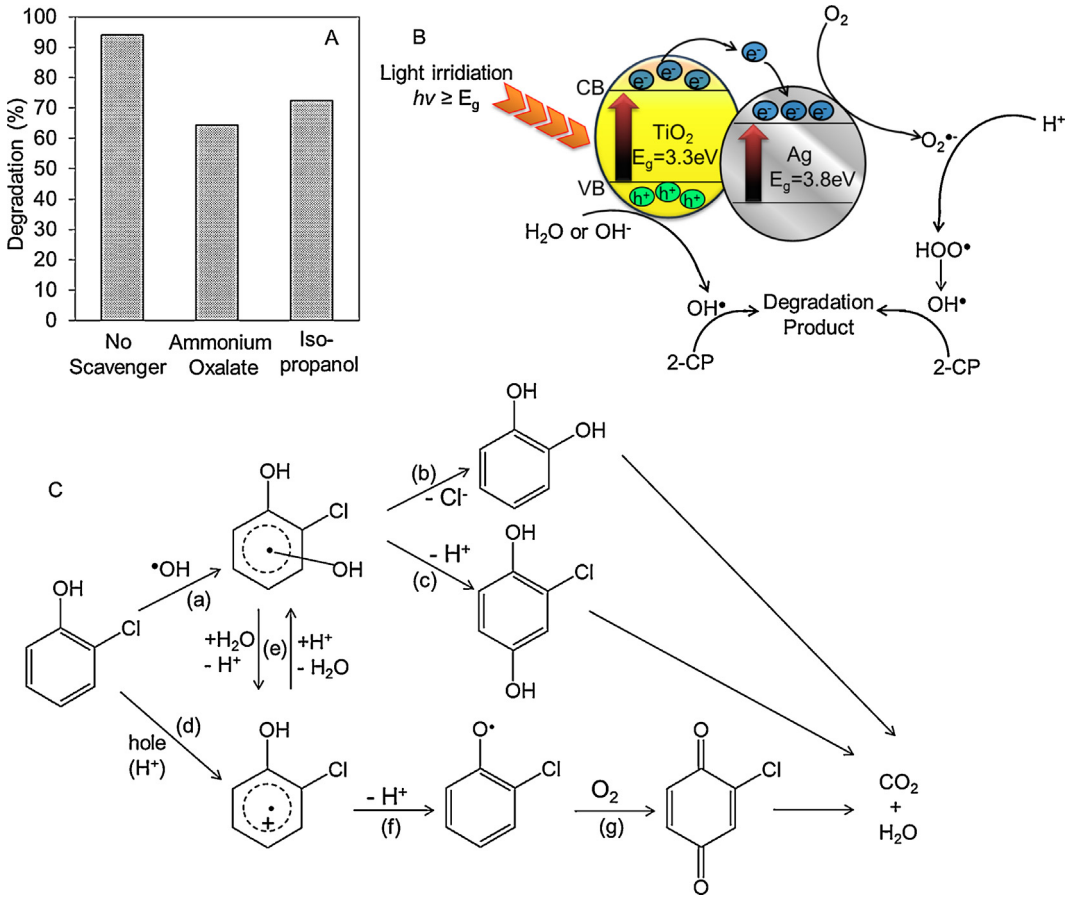

Fig. 9. (A) Photodegradation efficiencies of 2-CP in the presence of hole scavenger and •OH scavenger using 5 wt% Ag–TiO_2; (B) proposed mechanism of Ag–TiO_2 for photocatalytic reaction; and (C) proposed mechanism pathway for degradation of 2-CP ($C_{2\text{-CP}}$ = 10 mg L^{-1}, pH = 5, W = 0.375 g L^{-1}, t = 6 h, 30 °C).

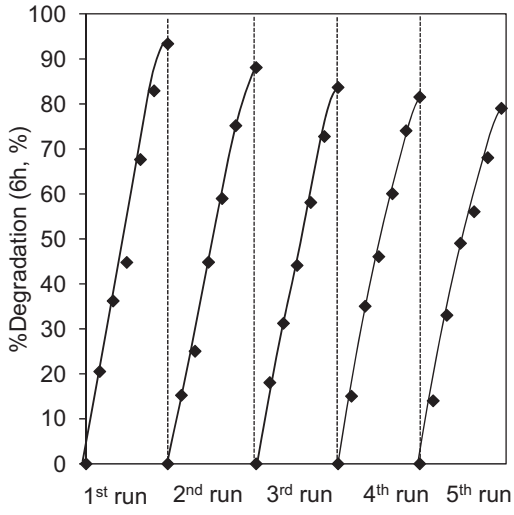

Fig. 10. Regeneration study of 5 wt% Ag–TiO_2 on degradation of 2-CP ($C_{2\text{-CP}}$ = 10 mg L^{-1}, pH = 5, W = 0.375 g L^{-1}, t = 6 h, 30 °C).

VB were positive enough to oxidize water or absorbed OH^- on the TiO_2 surface to generate $OH^•$ that degrades the 2-CP.

According to the literature [62], the degradation of 2-CP involved several steps and the mechanism is proposed as in Fig. 9C. The addition of $OH^•$ to the aromatic moiety (a) led to a formation of chlorodihydroxycyclohexadienyl radical (CIDHCHD). The introduction of $OH^•$ to ortho position followed by Cl-abstraction (b) resulted in catechol, while introduction to para position followed by H-abstraction (c) led to 2-chlorohydroquinone. Besides, direct reaction of 2-CP with the hole (d) generated a positive radical, which then converted into CIDHCHD after nucleophilic water addition (e), or chlorophenoxyl radical after deprotonation (f). Next, the chlorophenoxyl formed a quinonic derivative in the presence of dissolved O_2 (g). The subsequent aromatic intermediates from b, c and g underwent further oxidation to produce ring opening and aliphatic products such as carboxylic acid, which then finally led to total degradation of 2-CP to CO_2 and H_2O.

3.2.6. *Regeneration of the catalyst*

A series of repeat experiment was carried out to investigate the stability of the 5 wt% Ag–TiO_2 in the photodegradation of 2-CP (Fig. 10). It was determined that after five repetitions the catalyst was still active with only a slight decrease in the percent degradation from 93.3% to 79%. The decrease in photocatalytic efficiency may be due to the heat treatment, which causes the catalyst to aggregate and thus results in a decrease in its surface area [63]. Hence, it can be stated that the 5 wt% Ag–TiO_2 is quite stable as a photocatalyst and did not deactivate during degradation.

4. Conclusion

In conclusion, Ag^0 nanoparticles supported on a TiO_2 catalyst was prepared by a direct in situ electrochemical method which operated under mild conditions. The physicochemical properties of the Ag–TiO_2 were studied using XRD, FT-IR, Raman, UV–vis DRS, photoluminescence, surface area analysis, TEM, FESEM-EDX and cyclic voltammetry. The XRD, FT-IR, Raman and surface area analyses verified that Ag^0 as well as incorporated Ti—O—Ag species were formed on the TiO_2 structure. The bare TiO_2, and 1, 5 and 10 wt% Ag–TiO_2 gave 62, 75, 94, and 78% of photodegradation of 2-CP, respectively. The amount of distributed Ag^0 as well as oxygen vacancies on the surface of TiO_2 seemed to play important roles in the degradation that affected the electron–hole separation rate. Thus, the 5 wt% Ag–TiO_2 which has the highest content of Ag^0 as well as the greatest number of surface oxygen vacancies attaining the highest degradation. For the case of 10 wt% Ag–TiO_2, the longer the electrolysis time, the more isomorphous substitution occurred to form additional Ti—O—Ag bonds while decreasing the amount of Ag^0 and number of oxygen vacancies on the surface of the TiO_2, thus reduced the degradation efficiency. The kinetics studies demonstrated that the photodegradation of 2-CP followed a pseudo-first order Langmuir–Hinshelwood model where adsorption was the controlling step in the process. The regenerated photocatalyst was still stable after five cycling runs. It is believed that this direct in situ preparation method of metal could contribute to the synthesis of any catalyst for various applications, particularly for photocatalytic degradation of various organic pollutants.

Acknowledgments

The authors are grateful for the financial support by the Fundamental Research Grant Scheme (4F161), awards of MyPhD Scholarship (Nur Farhana Jaafar) from the Ministry of Higher Education Malaysia and to the Hitachi Scholarship Foundation for their support.

Appendix A. Supplementary data

Supplementary data associated with this article can be found, in the online version, at http://dx.doi.org/10.1016/j.apsusc.2015.02.106.

References

[1] J. Ananpattarachai, P. Kajitvichyanukul, S. Seraphin, Visible light absorption ability and photocatalytic oxidation activity of various interstitial N-doped TiO_2 prepared from different nitrogen dopants, J. Hazard. Mater. 168 (2009) 253–261.
[2] D. Gryglik, J.S. Miller, S. Zedakowicz, Singlet molecular oxygen application for 2-chlorophenol removal, J. Hazard. Mater. 146 (2007) 502–507.
[3] V.K. Gupta, A. Mittal, L. Krishnan, J. Mittal, Adsorption treatment and recovery of the hazardous dye, Brilliant Blue FCF, over bottom ash and de-oiled soya, J. Colloid Interface Sci. 293 (2006) 16–26.
[4] M. Pera-Titus, V. García-Molina, M.A. Baños, J.S. Esplugas, Degradation of chlorophenols by means of advanced oxidation processes: a general review, Appl. Catal. B 47 (2004) 219–256.
[5] S.K. Srivastava, V.K. Gupta, M.K. Dwivedi, S. Jain, Caesium PVC-crown (dibenzo-24-crown-8) based membrane sensor, Anal. Proc. 32 (1) (1995) 21–23.
[6] V.K. Gupta, M.A. Khayat, A.K. Singh, M.K. Pal, Nano level detection of Cd(II) using poly(vinyl chloride) based membranes of Schiff bases, Anal. Chim. Acta 634 (2009) 36–43.
[7] M.Z. Khan, P.K. Mondal, S. Sabir, Bioremediation of 2-chlorophenol containing wastewater by aerobic granules-kinetics and toxicity, J. Hazard. Mater. 190 (2011) 222–228.
[8] V.K. Gupta, I. Ali, V.K. Saini, Defluoridation of wastewaters using waste carbon slurry, Water Res. 41 (2007) 3307–3316.
[9] V.K. Gupta, A. Rastogi, Biosorption of hexavalent chromium by raw and acid-treated green alga *Oedogonium hatei* from aqueous solutions, J. Hazard. Mater. 163 (2009) 396–402.
[10] S. Yi, J. Cui, S. Li, L. Zhang, D. Wang, Y. Lin, Enhanced visible-light photocatalytic activity of Fe/ZnO for rhodamine B degradation and its photogenerated charge transfer properties, Appl. Surf. Sci. 319 (2014) 230–236.
[11] R. Jusoh, A.A. Jalil, S. Triwahyono, A. Idris, S. Haron, N. Sapawe, N.F. Jaafar, N.W.C. Jusoh, Synthesis of reverse micelle α-FeOOH nanoparticles in ionic liquid as an only electrolyte: inhibition of electron–hole pair recombination for efficient photoactivity, Appl. Catal. A 469 (2014) 33–44.
[12] V.K. Gupta, R. Jain, S. Varshney, Electrochemical removal of the hazardous dye Reactofix Red 3 BFN from industrial effluents, J. Colloid Interface Sci. 312 (2007) 292–296.
[13] V.K. Gupta, R. Jain, A. Mittal, M. Mathur, S. Sikarwar, Photochemical degradation of the hazardous dye Safranin-T using TiO_2 catalyst, J. Colloid Interface Sci. 309 (2007) 464–469.
[14] N.W.C. Jusoh, A.A. Jalil, S. Triwahyono, H.D. Setiabudi, N. Sapawe, M.A.H. Satar, A.H. Karim, N.H.N. Kamarudin, R. Jusoh, N.F. Jaafar, N. Salamun, J. Efendi, Sequential desilication–isomorphous substitution route to prepare mesostructured silica nanoparticles loaded with ZnO and their photocatalytic activity, Appl. Catal. A 468 (2013) 276–287.

[15] R. Saravanan, V.K. Gupta, V. Narayanan, A. Stephen, Visible light degradation of textile effluent using novel catalyst ZnO/γ-Mn_2O_3, J. Taiwan Inst. Chem. E 45 (2014) 1910–1917.
[16] R. Saravanan, H. Shankar, T. Prakash, V. Narayanan, A. Stephen, ZnO/CdO composite nanorods for photocatalytic degradation of methylene blue under visible light, Mater. Chem. Phys. 125 (2011) 277–280.
[17] H. Liu, L. Deng, C. Sun, J. Li, Z. Zhu, Titanium dioxide encapsulation of supported Ag nanoparticles on the porous silica bead for increased photocatalytic activity, Appl. Surf. Sci. 326 (2015) 82–90.
[18] L. Chen, T. Tran, T.C. Huang, J. Li, L. Yuan, Q. Cai, Synthesis and photocatalytic application of Au/Ag nanoparticle-sensitized ZnO films, Appl. Surf. Sci. 273 (2013) 82–88.
[19] R. Saravanan, N. Karthikeyan, V.K. Gupta, E. Thirumal, P. Thangadurai, V. Narayanan, A. Stephen, ZnO/Ag nanocomposite: an efficient catalyst for degradation studies of textile effluents under visible light, Mater. Sci. Eng. C 33 (2013) 2235–2244.
[20] J. Tian, R. Liu, G. Wang, Y. Xu, X. Wang, H. Yu, Dependence of metallic Ag on the photocatalytic activity and photoinduced stability of Ag/AgCl photocatalyst, Appl. Surf. Sci. 319 (2014) 324–331.
[21] A.A. Ismail, Facile synthesis of mesoporous Ag-loaded TiO_2 thin film and its photocatalytic properties, Microporous Mesoporous Mater. 149 (2012) 69–75.
[22] Y. Xu, H. You, TiO_2 modified with Ag nanoparticles synthesized via ultrasonic atomization-UV reduction and the use of kinetic models to determine the acetic acid photocatalytic degradation, Appl. Surf. Sci. 321 (2014) 481–487.
[23] R. Adhikari, G. Gyawali, T. Sekino, S.W. Lee, Microwave assisted hydrothermal synthesis of Ag/AgCl/WO_3 photocatalyst and its photocatalytic activity under simulated solar light, J. Solid State Chem. 197 (2013) 560–565.
[24] A.A. Jalil, M.A.H. Satar, S. Triwahyono, H.D. Setiabudi, N.H.N. Kamarudin, N.F. Jaafar, N. Sapawe, R. Ahamad, Tailoring the current density to enhance photocatalytic activity of CuO/HY for decolorization of malachite green, J. Electroanal. Chem. 701 (2013) 50–58.
[25] N. Sapawe, A.A. Jalil, S. Triwahyono, S.H. Adam, N.F. Jaafar, M.A.H. Satar, Isomorphous substitution of Zr in the framework of aluminosilicate HY by an electrochemical method: evaluation by methelene blue decolorization, Appl. Catal. B 125 (2012) 311–323.
[26] N. Sapawe, A.A. Jalil, S. Triwahyono, R.N.R.A. Sah, N.W.C. Jusoh, N.H.H. Hairom, J. Efendi, Electrochemical strategy for grown ZnO nanoparticles deposited onto HY zeolite with enhanced photodecolorization of methylene blue: effect of the formation of Si O Zn bonds, Appl. Catal. A 456 (2013) 144–158.
[27] N. Sapawe, A.A. Jalil, S. Triwahyono, One-pot electro-synthesis of ZrO_2–ZnO/HY nanocomposite for photocatalytic decolorization of various dye-contaminants, Chem. Eng. J. 225 (2013) 254–265.
[28] N.F. Jaafar, A.A. Jalil, S. Triwahyono, M.N.M. Muhid, N. Sapawe, M.A.H. Satar, H. Asaari, Photodecolorization of methyl orange over α-Fe_2O_3-supported HY catalysts: the effects of catalyst preparation and dealumination, Chem. Eng. J. 191 (2012) 112–122.
[29] A.A. Jalil, S. Triwahyono, N.A.M. Razali, N.H.H. Hairom, A. Idris, M.N.M. Muhid, A. Ismail, N.A.M. Yahaya, N.A.L. Ahmad, H. Dzinun, Complete electrochemical dechlorination of chlorobenzenes in the presence of various arene mediators, J. Hazard. Mater. 174 (2010) 581–585.
[30] A.A. Jalil, N. Kurono, M. Tokuda, Facile synthesis of ethyl 2-arylpropenoates by cross-coupling reaction using electrogenerated highly reactive zinc, Tetrahedron 58 (2002) 7477–7484.
[31] T. Nanba, S. Masukawa, J. Uchisawa, A. Obuchi, Influence of TiO_2 crystal structure on acrylonitrile decomposition over Ag/TiO_2, Appl. Catal. A 419–420 (2012) 49–52.
[32] C. Durucan, B. Akkopru, Effect of calcination on microstructure and antibacterial activity of silver-containing silica coating, J. Biomed. Mater. Res. B 93B (2) (2010) 448–458.
[33] A.B. Patil, K.R. Patil, S.K. Pardeshi, Enhancement of oxygen vacancies and solar photocatalytic activity of zinc oxide by incorporation of non-metal, J. Solid State Chem. 184 (2011) 3273–3279.
[34] R. Saravanan, V.K. Gupta, T. Prakash, V. Narayanan, A. Stephen, Synthesis, characterization and photocatalytic activity of novel Hg doped ZnO nanorods prepared by thermal decomposition method, J. Mol. Liq. 178 (2013) 88–93.
[35] S. Anandan, P.S. Kumar, N. Pugazhenthiran, J. Madhavan, P. Maruthamuthu, Effect of loaded silver nanoparticles on TiO_2 for photocatalytic degradation of Acid Red 88, Sol. Energy Mater. Sol. C 92 (2008) 929–937.
[36] R. Saravanan, H. Shankar, T. Prakash, V. Narayanan, A. Stephen, ZnO/CdO composite nanorods for photocatalytic degradation of methylene blue under visible light, Mater. Chem. Phys. 125 (2011) 277–280.
[37] R. Saravanan, S. Karthikeyan, V.K. Gupta, G. Sekaran, V. Narayanan, A. Stephen, Enhanced photocatalytic activity of ZnO/CuO nanocomposite for the degradation of textile dye on visible light illumination, Mater. Sci. Eng. C 33 (2013) 91–98.
[38] J. Yang, H. Bai, X. Tan, J. Lian, IR and XPS investigation of visible-light photocatalysis: nitrogen carbon-doped TiO_2 film, Appl. Surf. Sci. 253 (2006) 1988–1994.
[39] P. Falaras, A.H. Goff, M.C. Bernard, A. Xagas, Characterization by resonance Raman spectroscopy of sol–gel TiO_2 films sensitized by the $Ru(PPh_3)_2(dcbipy)Cl_2$ complex for solar cells application, Sol. Energy Mater. Sol. C 64 (2000) 167–184.
[40] R. Vinu, G. Madras, Photocatalytic activity of Ag-substituted and impregnated nano-TiO_2, Appl. Catal. A 366 (2009) 130–140.
[41] C. Su, L. Liu, M. Zhang, Y. Zhang, C. Shao, Fabrication of Ag/TiO_2 nanoheterostructures with visible light photocatalytic function via a solvothermal approach, Cryst. Eng. Commun. 14 (2012) 3989–3999.
[42] K.A. Bosnick, Raman studies of mass-selected metal clusters (Ph.D. thesis), Department of Chemistry, University of Toronto, 2000.
[43] W. Zhou, H. Liu, J. Wang, D. Liu, G. Du, J. Cui, Ag_2O/TiO_2 nanobelts heterostructure with enhanced ultraviolet and visible photocatalytic activity, Appl. Mater. Interfaces 2 (8) (2010) 2385–2392.
[44] R.N. Goyal, V.K. Gupta, M. Oyama, N. Bachheti, Voltammetric determination of adenosine and guanosine using fullerene-C60-modified glassy carbon electrode, Talanta 71 (2007) 1110–1117.
[45] A.H. Karim, A.A. Jalil, S. Triwahyono, N.H.N. Kamarudin, A. Ripin, Influence of multi-walled carbon nanotubes on textural and adsorption characteristics of in situ synthesized mesostructured silica, J. Colloid Interface Sci. 421 (2014) 93–102.
[46] V.K. Gupta, R. Jain, S. Varshney, Removal of Reactofix golden yellow 3 RFN from aqueous solution using wheat husk – an agricultural waste, J. Hazard. Mater. 142 (2007) 443–448.
[47] V.K. Gupta, A. Mittal, L. Kurup, J. Mittal, Adsorption of a hazardous dye, erythrosine, over hen feathers, J. Colloid Interface Sci. 304 (2006) 52–57.
[48] V.K. Gupta, A. Rastogi, A. Nayak, Adsorption studies on the removal of hexavalent chromium from aqueous solution using a low cost fertilizer industry waste material, J. Colloid Interface Sci. 342 (2010) 135–141.
[49] I.K. Konstantinou, T.A. Albanis, TiO_2-assisted photocatalytic degradation of azo dyes in aqueous solution: kinetic and mechanistic investigations: a review, Appl. Catal. B 49 (1) (2004) 1–14.
[50] K. Porkodi, V.K. Kumar, Comment on "Photocatalytic properties of TiO_2 modified with platinum and silver nanoparticles in the degradation of oxalic acid in aqueous solution" Langmuir Hinshelwood kinetics – a theoretical study, Appl. Catal. B 79 (2008) 108–109.
[51] C. Su, C. Shao, Y. Liu, Electrospun nanofibers of TiO_2/CdS heteroarchitectures with enhanced photocatalytic activity by visible light, J. Colloid Interface Sci. 359 (2011) 220–227.
[52] M.M. Joshi, N.K. Labhsetwar, P.A. Mangrulkar, S.N. Tijare, S.P.S. Kamble, S. Rayalu, Visible light induced photoreduction of methyl orange by N-doped mesoporous titania, Appl. Catal. A 357 (2009) 26–33.
[53] Y. Zhao, C. Li, X. Liu, F. Gu, H.L. Du, L. Shi, Zn doped TiO_2 nanoparticles with high photocatalytic activity synthesized by hydrogen–oxygen diffusion flame, Appl. Catal. B 79 (2008) 208–215.
[54] L. Sun, D. Zhao, Z. Song, C. Shan, Z. Zhang, B. Li, D. Shen, Gold nanoparticles modified ZnO nanorods with improved photocatalytic activity, J. Colloid Interface Sci. 363 (2011) 175–181.
[55] M.F.A. Taleb, Adsorption and photocatalytic degradation of 2-CP in wastewater onto CS/$CoFe_2O_4$ nanocomposite synthesized using gamma radiation, Carbohydr. Polym. 114 (2014) 65–72.
[56] L.C. Juang, G.U. Semblante, S.J. You, S.H. Hong, Degradation of 2-chlorophenol using carbon nanotube/titanium oxide composite prepared by hydrothermal method, J. Taiwan Inst. Chem. E. 44 (2013) 432–437.
[57] J. Rashid, M.A. Barakat, R.M. Mohamedb, I.A. Ibrahim, Enhancement of photocatalytic activity of zinc/cobalt spinel oxides by doping with ZrO_2 for visible light photocatalytic degradation of 2-chlorophenol in wastewater, J. Photochem. Photobiol. A: Chem. 284 (2014) 1–7.
[58] S. Buzby, M.A. Barakat, H. Lin, C. Ni, S.A. Rykov, J.G. Chen, S. Ismat Shah, Visible light photocatalysis with nitrogen-doped titanium dioxide nanoparticles prepared by plasma assisted chemical vapor deposition, J. Vac. Sci. Technol. B 24 (2006) 1210–1214.
[59] J. Rashid, M.A. Barakat, S. Pettit, J.N. Kuhn, In VO_4/TiO_2 composite for visible light photocatalytic degradation of 2-chlorophenol in wastewater, Environ. Technol. 35 (17) (2014) 2153–2159.
[60] R. Saravanan, E. Thirumal, V.K. Gupta, V. Narayanan, A. Stephen, The photocatalytic activity of ZnO prepared by simple thermal decomposition method at various temperatures, J. Mol. Liq. 177 (2013) 394–401.
[61] M.H. Sung-Suh, J.R. Choi, H.J. Hah, S.M. Koo, Y.C. Bae, Comparison of Ag deposition effects on the photocatalytic activity of nanoparticulate TiO_2 under visible and UV light irradiation, J. Photochem. Photobiol. A 163 (2004) 37–44.
[62] I. Ilisz, A. Dombi, K. Mogyorósi, A. Farkas, I. Dékány, Removal of 2-chlorophenol from water by adsorption combined with TiO_2 photocatalysis, Appl. Catal. B 39 (2002) 247–256.
[63] M. Huang, C. Xu, Z. Wu, Y. Huang, J. Lin, J. Wu, Photocatalytic discolorization of methyl orange solution by Pt modified TiO_2 loaded on natural zeolite, Dyes Pigment 77 (2008) 327–334.